Applied Energy 148 (2015) 121–133

Contents lists available at ScienceDirect

Applied Energy

journal homepage: www.elsevier.com/locate/apenergy

Performance characterization and placement of a marine hydrokinetic turbine in a tidal channel under boundary proximity and blockage effects

Nitin Kolekar, Arindam Banerjee *

Department of Mechanical Engineering & Mechanics, Lehigh University, Bethlehem, PA 18015, United States

HIGHLIGHTS

- Solid and wake blockage on turbine explored using laboratory experiments and CFD.
- Close proximity of hydrokinetic turbine to free surface affects performance.
- Enhanced performance with decreasing tip clearance, maximum at half turbine radius.
- At low values of tip clearance, free surface drop modified upper bypass and wake.
- Blockage from wake modification dependent on tip clearance, rotor rpm and *TSR*.

ARTICLE INFO

Article history:
Received 20 November 2014
Received in revised form 7 March 2015
Accepted 9 March 2015

Keywords:
Hydrokinetic turbine
Blockage
Free surface
Wake

ABSTRACT

Marine hydrokinetic turbine, when operating in a shallow channel is subjected to the boundary proximity effects from a deformable free surface on top and the channel bottom. A close proximity of turbine to these boundaries modifies the flow-field around the turbine and affects device performance. Significant flow acceleration occurs in and around the turbine rotation plane; the magnitude of which depends on size of the turbine relative to the channel cross-section and is commonly referred to as solid blockage. In addition, the wake behind the turbine creates a restriction to the flow called wake blockage. We focus on unraveling the influence of boundary proximity and blockage on the turbine performance through coupled experimental and computational studies. The experiments were carried out in an open surface water channel with a three bladed, constant chord, untwisted marine hydrokinetic turbine submerged at different depths and performance was evaluated under various operating conditions. The findings were complimented by a steady state computational fluid dynamics study that was carried out to understand the effect of flow Reynolds number and solid blockage on the turbine performance. A reduction in tip-depth of immersion was observed to improve the turbine performance until it reached an optimum depth beyond which a reduction in performance was observed due to free surface interaction with wake and bypass region. A transient CFD analysis with volume of fluid approach was performed to incorporate free-surface and buoyancy effects and augment flow-field characterization behind the turbine in the wake, upper bypass, and lower bypass regions. For low tip clearance ratios, a significant drop (up to 5–10% of channel depth) in free surface was observed behind turbine with complex three dimensional flow structures that lead to a skewed wake affecting its expansion and restoration process.

1. Introduction

Unlike wind turbines, marine hydrokinetic turbines (MHkT) operate in a bounded flow environment where the flow is constrained between the free surface and the channel (river/sea) bed. In many cases, the channel depth for commercial scale MHkT installation is between 1.5*D* and 3*D* (where *D* is the turbine diameter) which leads to a blockage ratio (*B* = ratio of turbine area to channel area) greater than 0.1 [1]. Under such circumstances, the turbine is subjected to effects of solid blockage that modifies the flow-field around the turbine and hence affects its performance [2–4]. In addition, the rotational motion of the blades creates a low pressure, low velocity *wake* region behind the turbine; the rotating wake presents an additional restriction to the flow called wake blockage.

* Corresponding author at: Packard Laboratory, Lehigh University, Bethlehem, PA 18015-3085, United States. Tel.: +1 (610) 758 4099; fax: +1 (610) 758 6224.
E-mail address: arb612@lehigh.edu (A. Banerjee).

http://dx.doi.org/10.1016/j.apenergy.2015.03.052
0306-2619/

Collectively, these two blockage effects result in accelerated flow near the rotor plane which in turn yields a higher performance compared to a turbine operating in an unblocked environment [5–7]. Quantifying the wake recovery distance behind a MHkT is thus important for designing optimum locations for multiple devices in a farm environment. Although the problem appears to be similar to wind-farm design; important differences exist primarily due to the bounded flow environment which alters the mechanism of wake recovery. This invalidates usage of wind-farm models in which wake restoration takes place by absorbing energy from the atmospheric boundary layer which can be treated as an infinite ambient reservoir [8]. For MHkT, where a limited water depth is available, the wake is tightly restricted between channel bottom wall and free surface that limits free expansion in directions perpendicular to the bounding surfaces. Installation also plays a pivotal role; MHkT can either be bottom mounted on a pier anchored to the channel bed or can be supported from a floating platform moored to the channel bed [9]. In both cases, they are subjected to effects of boundary proximity of either the deformable free surface or the channel bed. Proximity of a turbine to the free surface presents additional complexity to flow structures and hence affects the turbine performance. The deformable free surface allows the water level to drop behind the turbine rotational plane [10]. Though the solid blockage is constant, the drop in free surface height and its deformation behind the turbine with the associated wake modifications are expected to influence the flow-field and hence turbine performance; the effects may vary significantly due to changes in effective flow conditions, operating *TSR* (ratio of blade flow speed to flow speed), Reynolds number (*Re* = ratio of inertial forces to viscous forces) and Froude number (*Fr* = ratio of characteristic flow velocity to gravitational wave velocity). The severity of this effect is expected to be function of various parameters including but not limited to blade shape (airfoil shape, chord and twist distribution), blade pitch angle, *TSR*, free surface proximity, channel wall proximity, and solid blockage itself.

An extensive literature review on wind-turbines was undertaken due to similarity in the working principle with MHkTs. Several experimental studies have been carried out for wind turbines in both unblocked and blocked flow environments to investigate the effects of tip speed ratio, Reynolds number, blade profile, velocity gradient that may exist across the rotor plane and turbulent wind characteristics [8,11–14]. However, the results are not directly applicable as MHkTs operate in a flow medium which is fundamentally different from wind turbines; denser working fluid leads to higher structural stresses on turbine blades [15,16]. In addition, MHkTs operating at higher rotational speeds and high angle of attack in a near free surface environment may get subjected to cavitation effects [15]. Several experimental studies have also been performed to quantify blockage effects on turbine performance. Majority of the early experimental work was done either in wind-tunnels or water channels with the aim of validation and verification of simple physics based models of such flows [2,11,12]. Chen and Liou [12] experimentally investigated effects of tunnel blockage on turbine performance. Blockage effect was quantified in terms of blockage factor by measuring tunnel flow velocity with and without turbine. The blockage factor was found to be strongly related to solid blockage, *TSR*, and blade pitch angle. Higher blockage effects were observed at higher solid blockage and higher *TSR* values. McTavish et al. [3] studied effect of blockage on initial wake expansion for different sized rotors in water channel using dye visualization technique. Higher blockage was found to narrow down the wake expansion and modify the vortex pairing behind the turbine. Several studies have also been performed to analyze free surface effect on marine current turbines; however, majority of these studies used a porous disc to replicate the turbine rotor. Myers and Bahaj [17] carried out experiments with mesh disks to study effect of disk proximity to sea bed/water surface on wake structures behind porous disks. Varying the disk proximity to sea/bed and water surface was found to affect wake structure and its recovery duration. Bahaj et al. [18] performed analytical and experimental study to investigate the effect of surface proximity on turbine performance. Their experiments in a cavitation tunnel and tow tank showed reduction in turbine power with decreasing blade tip-free surface clearance. Experimental investigations by Birjandi et al. [19] with a vertical axis hydrokinetic turbine reported improved performance with increasing free surface proximity. The presence of turbine in a tidal channel not only affects the downstream flow but also the flow upstream of the turbine. Experimental and computational investigations of Medici et al. [11] show influence of blockage on flow up to three turbine diameters upstream of the rotor plane. Near upstream flow showed three dimensional flow structures indicating effect of turbine geometry on incoming flow, similar to near wake flow.

Analytical models for characterizing the turbine performance are based on application of linear momentum theory. Garrett and Cummins [20] applied linear momentum theory for flow constrained between two rigid surfaces and found increase in turbine power with increasing blockage ratio. Houlsby et al. [21] used linear momentum theory to analyze a pressure constrained, parallel-sided tube scenario with an extension to open channel flow. A quartic equation was presented relating flow Froude number, blockage ratio, and flow speeds in wake and bypass region behind turbine. A similar analysis was presented by Whelan et al. [10] yielding a quartic equation relating above quantities. Analytical predictions were comparable with experimental data for mesh disc simulator and two bladed rotor in wind tunnel and water channel for different blockage conditions. Lartiga and Crawford [22] used actuator disc modeling with blockage corrections to predict the performance of tidal turbine in blocked environment. Flow field data from PIV measurements and CFD simulations were used to account for blockage effect. Analytical predictions were in good agreement at lower blockage ratio but showed significant deviations at higher blockage ratios. Computational study by Sun [23] with porous discs reported localized flow acceleration in region between wake and channel bottom. Free surface drop behind mesh disc was observed to affect wake characteristics and turbine performance as well. Consul et al. [4] investigated effect of blockage and free surface deformation on performance of a marine cross-flow turbine for different blockages and free surface boundary conditions using two-dimensional CFD modeling. The deformable free surface boundary condition lead to 6.7% performance improvement compared to closed lid condition due to higher effective blockage caused by free surface deformation. Froude number (over the range studied: 0.08–0.13) was reported to have very small effect on power coefficient (henceforth referred to as C_p = ratio of turbine power to water power) but significantly affected the free surface drop. Recently Bai et al. [24] performed numerical simulations using immersed boundary method to predict marine current turbine performance under free surface flow conditions and validated it with experimental data. No significant free surface deformation was reported with turbine operating with blade tip immersed $\sim 1 \times R$ below the free surface, where R denotes the turbine radius. Computational study by Zhou and Wang [25] investigated effect of Froude number, turbine diameter and depth of immersion on free surface wave induced by tidal turbine and its effect on turbine performance. But the computational study was not able to conclude on effect of depth of immersion on turbine performance. Lee et al. [26] used BEM and CFD based models for performance prediction of a horizontal axis tidal turbine. A new design was suggested with raked tip blades for better cavitation and acoustic performance. Though there is an increasing body of work focusing on experiments, computations and analytical

models to quantify blockage and free-surface effects on performance, majority of the experimental and computational studies model turbine as a porous mesh disc and analytical models are limited to actuator disc modeling [17,18,23,27].

To the knowledge of authors, there is no quantitative computational or experimental study exploring effect of blockage and wake-bypass flow interaction aiming to determine optimum depth of immersion for MHkT installations. We report results of computational and experimental investigations to quantify effect of blockage and boundary proximity on the performance of a three bladed MHkT. Experimental investigation are augmented by a flow field characterization with steady and transient computational fluid dynamics study. Three dimensional CFD with rotating reference frame technique was used to quantify effect of Reynolds number and blockage ratio on turbine performance characteristics. Transient CFD calculations for wake and free surface flow characterization take into account buoyancy effects and free surface effects using a volume of fluid (VOF) approach [28]. Experiments were carried out in an open surface water channel with a constant chord, zero twist hydrokinetic turbine under various operating conditions. Flow speed, rotational speed and turbine submerged depth were varied during the experiment to study their effects on turbine performance. Flow speed was varied from 0.5 m/s to 0.9 m/s to achieve different Froude numbers [0.20–0.37]. Further, to investigate effect of surface proximity, turbine submerged depth was varied so that blade tip to free surface clearance (h_U) is between 0.01 m and 0.22 m. This lead to turbine tip clearance ratios (δh_U) of 0.03–0.73 (see Fig. 1), which represents the ratio of water height above turbine rotation disc (h_U) up to free surface to the turbine diameter (D). Current experimental and computational investigations will enhance our limited understanding of flow-field around MHkT in its natural environment. Further, experimental investigations will provide useful means to quantify effect of boundary proximity on MHkT performance thereby facilitating MHkT site selection and deployment process.

2. Computational fluid dynamics

To understand the flow-field around a marine hydrokinetic turbine operating under various Reynolds number and boundary proximity conditions, a three dimensional CFD analysis was carried out using both steady state and transient solver schemes. Steady state analysis was carried out using multiple reference frame approach in CFX. More details about this technique can be found in [16,29,30]. A moving mesh technique was adapted for transient simulations for which inner domain containing turbine rotates at specified angular velocity during each time step until convergence for continuity and momentum equations is reached. The flow domain consisted of 3.5 million hybrid cells with prism layers on turbine surface for boundary layer resolution (Fig. 2). A grid convergence study was carried out by varying the mesh size from 1.5×10^6 cells to 4×10^6 cells and a mesh with 3.5 million cells

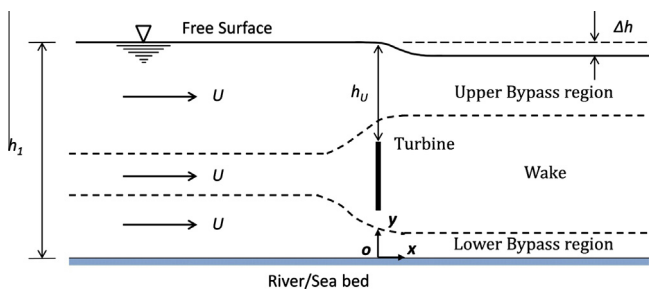

Fig. 1. Schematic of flow around MHkT in shallow river/tidal channel showing wake, upper bypass and lower bypass regions.

was found to be optimum from computational and accuracy standpoint which resulted in less than 5% variation in torque compared to a finer mesh of 4×10^6 cells. The mesh used for fluid domain is such that average y^+ (which defines distance of first mesh node from the wall) is 2.2 with y^+ ranging between ($0.1 \leqslant y^+ \leqslant 9$) for the highest flow speed and RPM case, i.e. $U = 0.9$ m/s, $TSR = 8$ that corresponds to tip speed velocity of 7.26 m/s. Reynolds averaged Navier–Stokes (RANS) equations were solved using $\kappa - \omega$ SST turbulence model for which, $y^+ \leqslant 10$ is acceptable for predicting boundary layer separation effects [31,32]. Fig. 2 shows schematic of fluid domain used during computations reported in this paper. The simulation domain was modeled to actual water channel test section of size 0.61 m × 0.61 m and 1.98 m long. A uniform velocity of 0.5 m/s was specified at the inlet. The channel outlet was specified outlet boundary condition with relative pressure of zero. The reference pressure for simulations was set to atmospheric pressure. The channel walls were modeled as no-slip walls and channel top is modeled as entrainment with zero relative opening pressure. With entrainment option at channel top surface, the flow direction is not specified but the flow solver locally calculates the flow direction based on flow velocity field. Buoyancy effects were modeled during transient simulations but were neglected for steady state analysis. The tunnel bottom was specified as a reference for gravity and hydrostatic pressure calculations along the channel depth. Transient simulations were carried out for flow velocity of 0.5 m/s and rotational speed of 200 RPM which corresponds to TSR (ratio of blade tip speed to flow speed) of 5.85. Time step was selected such that turbine rotated 2° during each time step which lead to average CFL (Courant–Friedrichs–Lewy condition) number of less than 5. CFL number defines a necessary condition for numerical stability of a hyperbolic partial equation. The restriction on CFL number depends on type of solver (discretization scheme) used for CFD analysis. For explicit solver, CFL < 1 provides good convergence, while for implicit solver higher values of CFL are acceptable. Current CFD analysis was performed with an implicit solver within CFX for which CFL < 5 was acceptable from numerical stability and expense standpoint [33]. Further, to ascertain the convergence with respect to time step size, an independence study was performed by varying time step size such that the turbine blade rotated 5°, 3°, 2° and 1° per time step. The difference between calculated power coefficients with respect to 2° case was 11%, 7%, 0% and 1.5% respectively. Thus a time step that corresponds to 2° rotation was chosen for current analysis considering numerical stability, accuracy and computational expenses. The fluid domain was initialized with a flow velocity of 0.5 m/s and turbulence intensity of 5% throughout the domain. In addition, the hydrostatic pressure at every point (and time step) in the domain was determined from density, volume fraction and hydrostatic head at that instant of time using a user defined function. The turbulence boundary conditions at inlet and outlet were specified as turbulence intensity of 5% and turbulent viscosity ratio of 10%. The convergence criteria for rms residuals of continuity, momentum, and turbulence quantities were set to 10^{-5}.

During transient simulation initial free surface height at the channel outlet is specified as 95% of the inlet height (5% free surface drop). This assumption was based on the blade element momentum calculations incorporating a quartic equation relating blockage ratio, Froude number, bypass flow and wake flow for current turbine prototype and operating conditions [10,14]. In addition, during experimentation, the free surface height at the channel exit was found to be dependent on flow speed, rotational speed and depth of immersion that varied from 1% to 5% of channel depth. Since the value of the free-surface drop is not known *a priori*, a value of 5% obtained from BEM predictions which also corresponds to the maximum drop measured during experimentation was used in all simulations. The dynamic variation of free surface

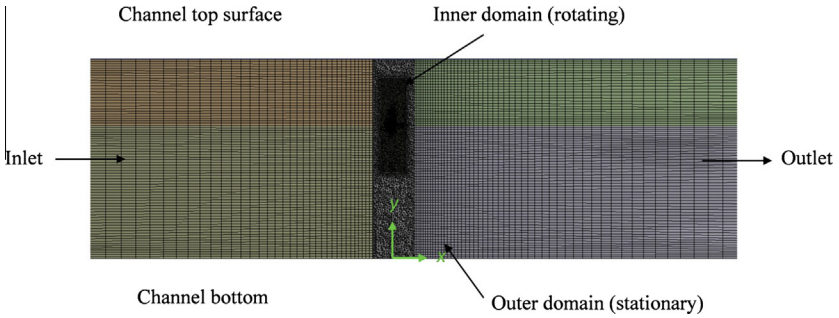

Fig. 2. Computational mesh used for CFD study.

height along the channel length (and width) is determined during transient simulations using VOF formulations. Free surface simulations were carried out in ANSYS CFX 15.0 using multiphase modeling with homogeneous model which uses VOF approach and is based on the concept of fluid volume fraction. A common flow field, temperature and turbulence field is shared by all fluids and for a given transport process, transported properties (except volume fraction) are assumed to be same for all phases [30]. The VOF model as developed by Hirt and Nichols [28] is based on Eulerian approach (volume-tracking) where fluid flows through a fixed mesh. The VOF method assumes that each control volume contains only one phase (water, air or interface between the two in this case) and solves only one set of momentum equation for all phases (Eq. (1))

$$\frac{\partial}{\partial t}(\rho u_j) + \frac{\partial}{\partial x_i}(\rho u_i u_j) = -\frac{\partial P}{\partial x_j} + \frac{\partial}{\partial x_j}\mu\left(\frac{\partial u_i}{\partial x_j} + \frac{\partial u_j}{\partial x_i}\right) + \rho g_j + F_j \qquad (1)$$

where u represents fluid velocity components, P is fluid pressure, μ represents effective fluid viscosity, ρ is fluid density, g is acceleration due to gravity, and F represents body forces. In this approach, actual interface is not tracked but in fact is reconstructed from other flow field properties like volume fraction. A step function (α) is used to define presence or absence of water within the computational domain. A value of 1 defines presence of water and value of zero defines presence of air within the control volume. The control volumes for which α are neither zero nor one represent the interface region between water and air. The tracking of the interface between the fluids is accomplished by solving volume fraction continuity equation for one of the phases (qth phase in Eq. (2)).

$$\frac{1}{\rho_q}\left[\frac{\partial}{\partial t}(\alpha_q \rho_q) + \nabla.(\alpha_q \rho_q \vec{v}_q) = \sum_{p=1}^{n} \dot{m}_{pq} - \dot{m}_{qp}\right] \qquad (2)$$

where $\dot{m}_{qp}$ is the mass transfer from phase q to phase p and $\dot{m}_{pq}$ is mass transfer from phase p to phase q. It was assumed that the interface between the two phases remain distinct and well defined so that air does not get entrained into water.

3. Facility, experimental set-up and model prototype

All experiments were carried out in an open surface recirculating water channel at Lehigh University with a test cross-section size of 0.61 m × 0.61 m and length of 1.98 m (Engineering Laboratory Design, USA). This facility is equipped with a 25HP single stage axial flow propeller pump with maximum discharge of 5590 gallons per minute. The propeller pump RPM and hence the test section flow velocity is controlled and regulated through a transistor inverter type variable frequency controller (Toshiba Model VFAS1-2185PM-HN). Flow velocity can be varied from 0.03 m/s to 0.94 m/s and can be measured within an accuracy of ±2%. The flow quality is such that the turbulence intensity is maintained to a value of less than 1%.

3.1. Turbine prototype

The model prototype used for current study is a three bladed, 0.14 m radius (R), zero twist, constant chord (0.01676 m) blade turbine made from corrosion resistant aluminum alloy (Fig. 3). Turbine blades are formed from SG6043 airfoil on a five-axis CNC machine. Turbine blades are held together inside a two-part hub and their orientation can be changed to adjust blade pitch to desired angle. To limit the number of independent variable to minimum, all experimental runs were performed with turbine blades oriented at 10° blade pitch. The turbine prototype when operated in our facility leads to area based blockage ratio of 16.5%.

3.2. Experimental setup

The experimental setup (see Fig. 4) consisted of a lab scale model hydrokinetic turbine attached to a horizontal shaft, driven by a stepper motor which maintains a precise rotational velocity through a micro-stepping driver and controller mechanism. The stepper motor used for current study was NEMA23 series, 24VDC motor with resolution of 1600 micro-steps per revolutions. The stepper motor was connected to the turbine shaft through a flexible coupling. The motor and flexible coupling were enclosed inside a watertight acrylic cylinder, which was then connected to a thrust torque sensor (Model # TFF400, Futek Inc.). The acrylic cylinder was continuously pressured/purged to avoid water leakage into the system. Finally, the reaction torque-thrust sensor was fixed to a vertical post, which was connected to a horizontal frame supported at channel top. The vertical post can be raised/lowered inside the water channel to vary the free surface proximity of turbine. During experimental run, data from torque-thrust sensor was continuously monitored and acquired on a desktop computer at high sampling rate of 500 samples/s for further analysis. According to manufactures specifications, the torque/thrust sensor was accurate to within ±1% for current measurement range which was also confirmed by in-house calibration. A single sample uncertainty analysis for U, RPM, and torque based on Kline and McClintock [34] showed maximum uncertainty of 1% on TSR and 3% on C_p calculations.

4. Results and discussion

Results from experimental and computational investigations carried out on a constant chord, untwisted three bladed MHkT are discussed. Experiments were carried out with turbine operating at various flow velocities and immersion depths over a range of TSR values. Experimental data is compared with CFD results for three flow velocities (0.5 m/s, 0.73 m/s and 0.9 m/s) for validation purpose. Upon validation, the CFD technique was extended to investigate effect of blockage ratio and flow velocity on turbine performance. CFD analysis is carried out for various sized flow

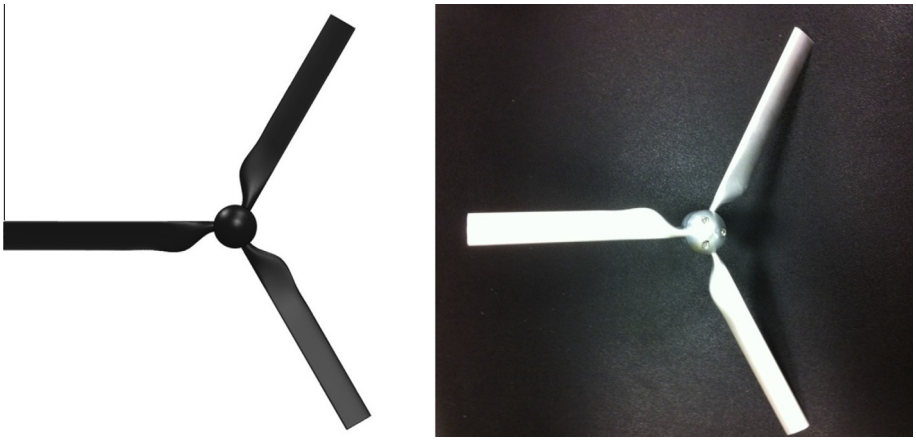

Fig. 3. CAD model and photograph of turbine prototype used for current study.

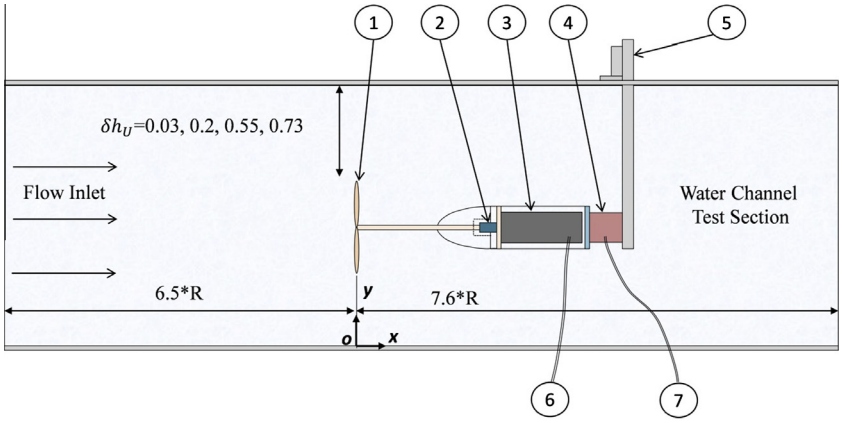

1 – Turbine, 2 – Flexible Coupling, 3 – Motor, 4 – Thrust-Torque Sensor,
5 – Support Structure, 6 – To Motor Controller, 7 – To Data Logging

Fig. 4. Schematic of experimental set-up [R = 0.14 m].

domains to model different blockage conditions. The effect of Reynolds number on the turbine performance was investigated by subjecting the turbine to flows with various inflow velocity conditions at domain inlet. Experimental runs in addition to the validation cases were performed with turbine operating at various depths of immersions to analyze the effect of boundary proximity (deformable free surface and non-erodible channel bottom wall) on turbine performance in an attempt to determine an optimum submersion depth that corresponds to a maximum power coefficient for the turbine.

4.1. Validation of CFD technique

Fig. 5 presents a comparison between experimental data and steady state CFD predictions for various flow velocities. During experimentation, turbine was submerged such that its axis was at the central height of channel and turbine performance was measured at flow velocities of 0.5 m/s, 0.73 m/s, and 0.9 m/s over a range of *TSR* values which correspond to turbine diameter based Reynolds number of 1.4×10^5, 2.0×10^5, and 2.5×10^5 respectively. For a *TSR* of 5, these flow speeds correspond to Reynolds numbers of 4.1×10^4, 6×10^4, and 7.4×10^4 respectively based on chord length and flow velocity at blade tip. Froude number based on total channel depth (upstream the turbine) for these flow velocities were 0.2, 0.3, and 0.37 respectively. For each flow speed, the rotational speed was varied from 30 to 300 revolutions per minute (RPM) and torque values were recorded from submerged torque-thrust sensor at sampling rate of 500 samples per second. As the flow speed increases from 0.5 m/s to 0.73 m/s, so does the turbine performance. This can be attributed to higher lift forces on turbine blades due to increase in Reynolds number (based on chord and effective velocity at blade tip) from 4.1×10^4 to 6×10^4. However, increasing flow velocity (U) from 0.73 m/s to 0.9 m/s did not cause any appreciable change in C_p vs. *TSR* curve (compare Fig. 5b and c) suggesting that turbine performance is weakly sensitive to Reynolds number effect beyond U = 0.73 m/s for the range of Reynolds numbers considered in the current study.

Another aspect of improvement in performance with flow velocity is related to increase in Froude number which defines the relation between relative flow velocity and gravitational flow speed. Higher the flow velocity compared to gravitational flow speed (which is a function of channel depth), higher the Froude number. This change in Reynolds and Froude number is associated with flow field modification in near downstream and near upstream regions of turbine and hence affects the turbine performance.

For flow velocity of 0.5 m/s, in addition to actual measured experimental data, a corrected curve is added considering assumed system efficiency of 10% to account for losses due to friction and torque transmission form turbine to reaction torque sensor. From

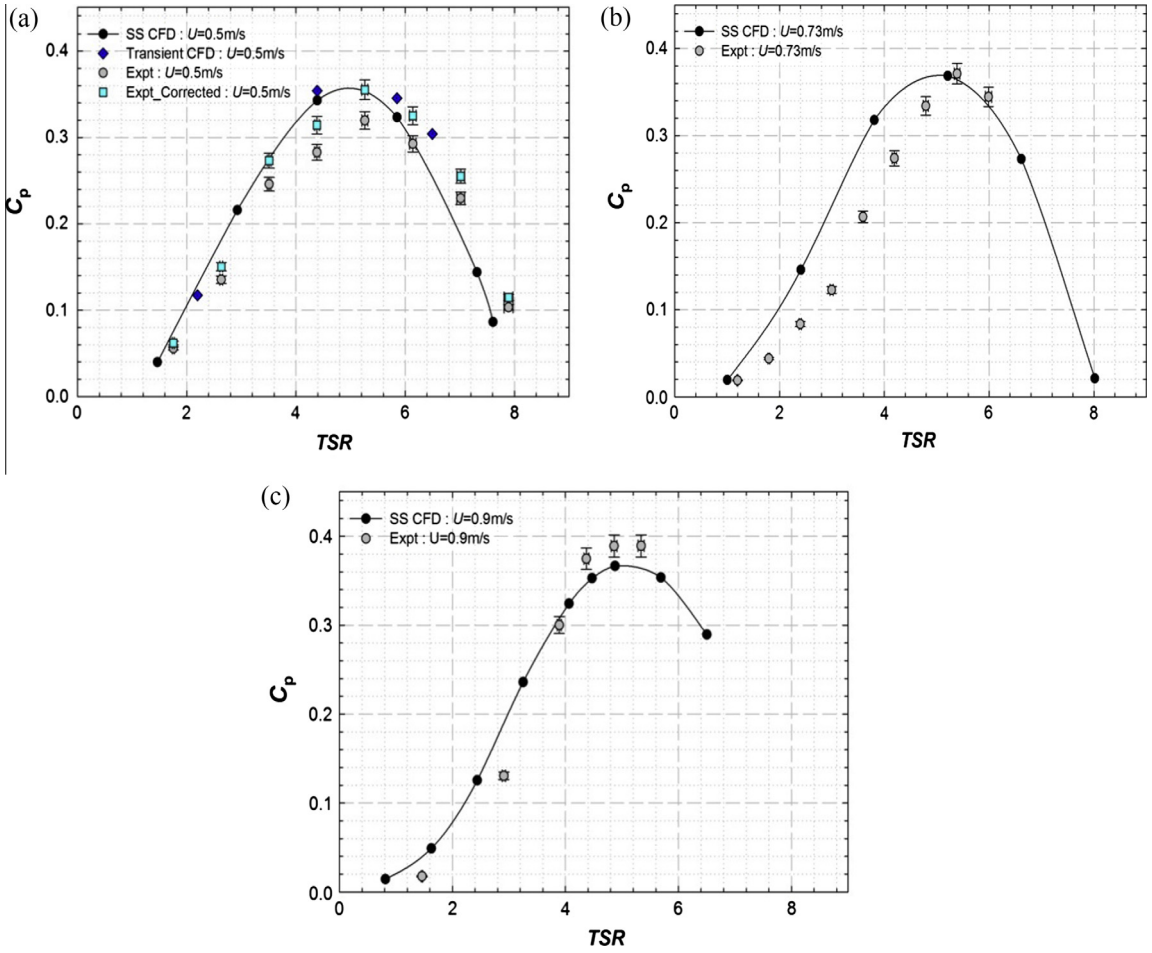

Fig. 5. Comparison of experimental data with steady state (SS) CFD results for (a) $U = 0.5$ m/s, (b) $U = 0.73$ m/s and (c) $U = 0.9$ m/s (vertical and horizontal error bars represent uncertainty in C_p and *TSR* measurements respectively), blue diamonds in figure (a) represent predictions from transient CFD. (For interpretation of the references to color in this figure legend, the reader is referred to the web version of this article.)

Fig. 5, it follows that CFD tend to over-predict the performance at lower *TSR* values, but at higher rotational speeds (when blockage effects are high, as discussed in Section 4.3) experimental data shows higher C_p compared to CFD prediction. Further, it is to be noted that, CFD and experimental data curves for C_p vs. *TSR* for all flow velocities cross each-other at rotational speed around 200–250 RPM (*TSR* range of 4–6). The deviation in performance prediction can be attributed to absence of free surface and buoyancy modeling during steady state CFD analysis which modifies the flow field (and provides additional blockage) and hence the turbine performance. In addition, the implication of blockage effects is not only to increase the turbine performance but also to shift entire C_p vs. *TSR* curve (for experimental data) away from the origin (in east–north direction), thereby shifting the optimum performance to higher *TSR* value as can be seen in Fig. 5. The severity of this effect varies with flow speed and rotational speed as will be illustrated in Figs. 8 and 10 in the later part of this manuscript. These effects were modeled during transient CFD analysis as presented in Section 4.4.2. A flow speed of $U = 0.5$ m/s and *TSR* value of 5.85 was chosen for transient simulations, around which a good match was observed between CFD predictions and experimental data. The diamonds on Fig. 5a present C_p predictions form transient CFD that show higher values compared to steady CFD and show better agreement with corrected experimental data. In spite of inability to model buoyancy and free surface effects, steady state CFD presented a computationally efficient approach for turbine performance characteristics prediction. It is to be noted that, the

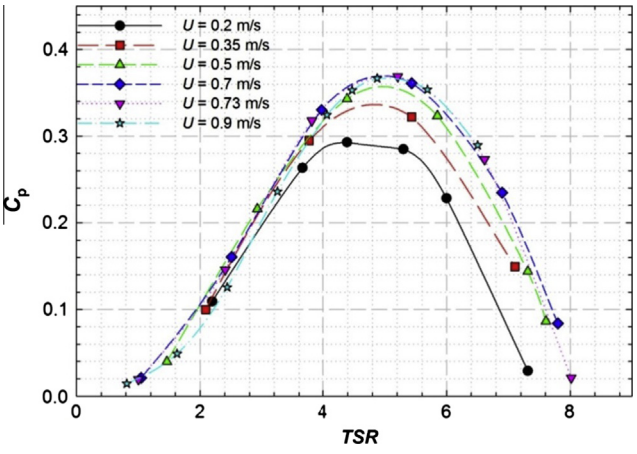

Fig. 6. Effect of flow velocity on turbine performance characteristics.

computational domain and turbine model are 1:1 replica of actual water channel and turbine prototype. This results in similar blockage effects for data-sets from both experiments and CFD modeling. Hence during CFD validation, blockage corrections were not applied to the experimental data. The effect of blockage on turbine performance is investigated separately and is reported in Section 4.3.

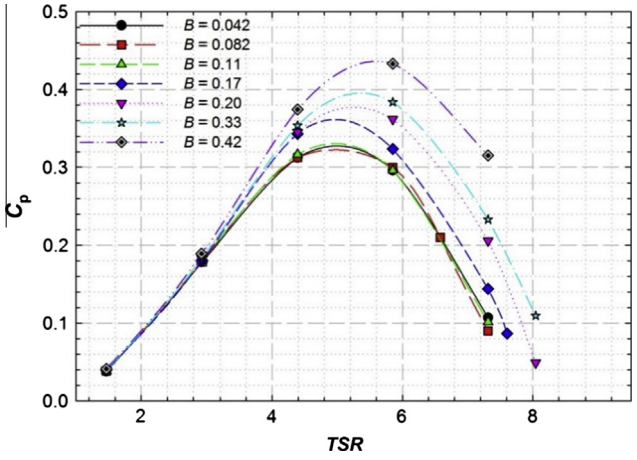

Fig. 7. Effect of blockage ratio on turbine performance characteristics.

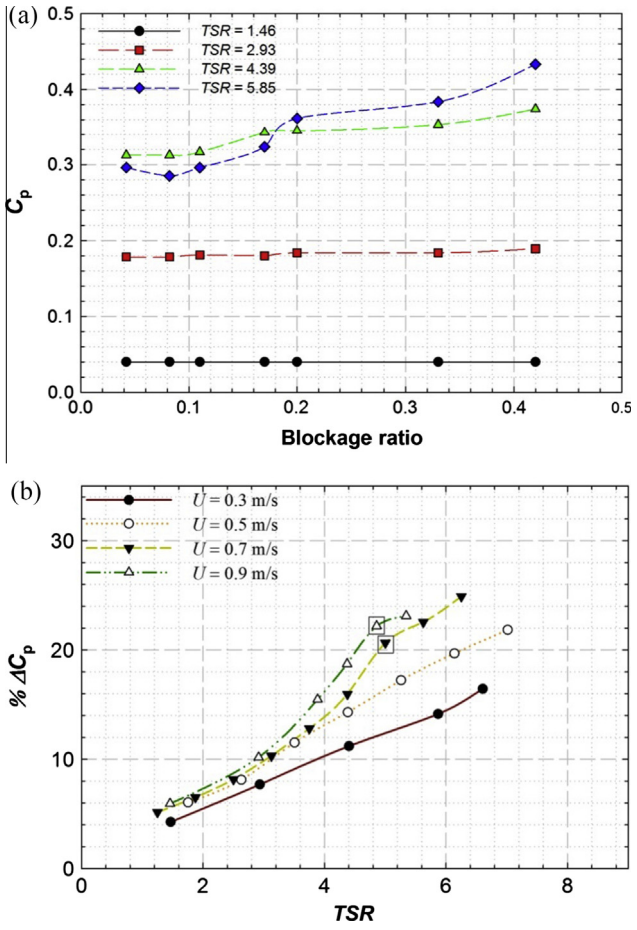

Fig. 8. Influence of *TSR* on blockage effect. (a) Variation of power coefficient with blockage ratio at various *TSR* values: CFD study; (b) effect of *TSR* on percentage increase in measured C_p (with respect to unblocked case) at various flow velocities: Experimental data.

4.2. Effect of Reynolds number on turbine performance characteristics

Though it is customary to express turbine performance characteristics in terms of non-dimensional parameters-*TSR* and C_p, one has to be cognizant of the fact that *TSR* does not represent actual flow velocity but is a ratio of blade tip velocity to flow velocity. Turbine blades are often made from airfoil sections whose lift and drag characteristics are strongly dependent on operating Reynolds number and hence flow velocity. A turbine when placed in tidal/river channel will be subjected to varying flow speeds, hence it is important to understand the effect of Reynolds number on its performance characteristics over a wide range of flow velocities. During the present study, a steady state CFD with rotating reference technique [16,29,30], validated with experimental data was used to understand effect of operating Reynolds number on turbine performance. CFD simulations were carried out for lab scale prototype in water channel sized fluid domain at flow velocities ranging from 0.1 m/s to 0.9 m/s. The results of variation of performance characteristics with flow velocity are presented in Fig. 6. With increasing flow velocity from 0.1 m/s, an improvement in turbine performance was observed with C_p vs. *TSR* curve reaching higher maxima and spreading over wider *TSR* range. The improvement trend continued until flow velocity reached 0.7 m/s above which no appreciable improvement was noticed. This corresponds to chord based Reynolds number of 1.2×10^4 and diameter based Reynolds number of 2.0×10^5 beyond which C_p vs. *TSR* curve became insensitive to Reynolds number changes at high *TSR* values (*TSR* > 5) but was weakly sensitive to Reynolds number changes at low *TSR* values.

4.3. Effect of blockage on turbine performance characteristics

The steady state CFD technique was used to investigate effect of blockage on turbine performance characteristics. The turbine geometry used for CFD analysis was a three bladed lab prototype of 0.14 m radius. Fluid domains of different cross-section sizes were created to achieve various (solid) blockage ratios in the range [0.042, 0.42]. The largest domain corresponds to test section of 1.22 m × 1.22 m and the smallest test section size corresponds to 0.38 m × 0.38 m, all other test sections have width of 0.61 m but height varying from 0.3 m to 1.22 m to achieve various blockage ratios. All simulations were carried out with channel inlet flow velocity of 0.5 m/s. Fig. 7 shows variation of turbine performance with *TSR* at various blockage ratios. For blockage ratios below 10%, no significant variation of performance characteristics was observed, thus no blockage corrections are necessary. Increasing the blockage ratio beyond 10% resulted in consistently higher performance with up to ~35% improvement in C_p for the case with 42% blockage when compared to the unblocked case. At lower *TSR* values (<4), the turbine performance was found to be weakly dependent on blockage ratio. But with increasing *TSR*, performance curves started deviating from each other showing stronger influence of blockage. Higher blockage ratios were found to increase torque on turbine resulting in improved performance.

The total blockage to which the turbine is subjected is combination of solid blockage and wake blockage [5,6] and changes with turbine rotational speed. Higher rotational speed represents faster rotating wake resulting in stronger wake blockage effect. To get a better insight into effect of turbine rotational speed on blockage effect, data set from steady CFD analysis are plotted in Fig. 8a such that the *y*-axis represents the turbine performance and the *x*-axis represents solid blockage. Lines of constant *TSR* values: 1.46, 2.93, 4.39 and 5.85, are plotted and compared. At lower *TSR* value (1.46), blockage does not seem to have any effect on C_p. This is due to the fact that, at low rotational speeds, turbine blades experience high relative angle of attack that causes flow separation on blades. An increase in blockage leads to larger effective flow velocity further increasing the relative angle of attack. This worsens the flow separation on turbine blades, adversely affecting its performance. Thus, blockage induces competing phenomena of elevated velocity (which increases torque) and increased flow separation (which reduces torque). At low *TSR* values, the improvement in turbine performance due to elevated effective velocities is nullified by flow separation effects and blockage does not cause any appreciable

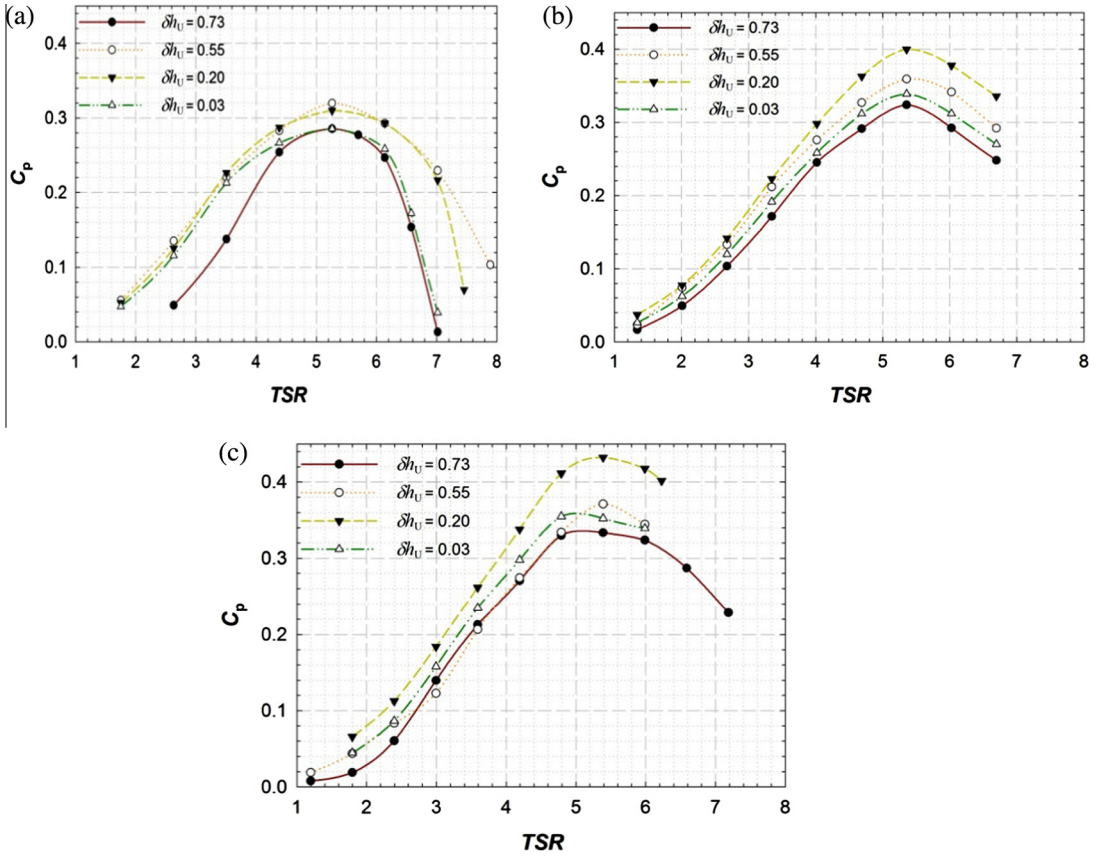

Fig. 9. Effect of free surface proximity on turbine performance at different flow velocities (a) $U = 0.5$ m/s, (b) $U = 0.66$ m/s and (c) $U = 0.73$ m/s.

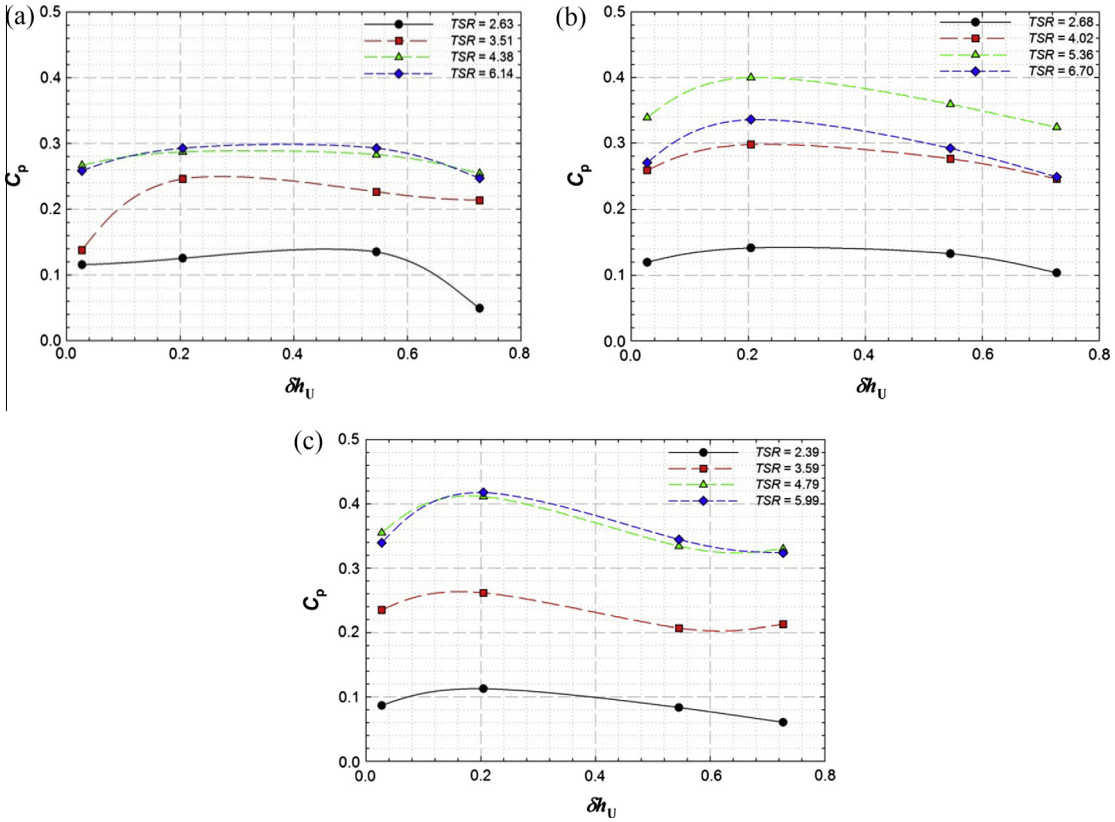

Fig. 10. Effect of Reynolds number on turbine performance characteristics at various operating *TSR* values and tip clearance ratios: (a) $U = 0.5$ m/s ($Re_D = 1.37 \times 10^5$), (b) $U = 0.66$ m/s ($Re_D = 1.8 \times 10^5$), and (c) $U = 0.73$ m/s ($Re_D = 2 \times 10^5$), where, Re_D is Reynolds number based on turbine diameter.

enhancement in power coefficient as illustrated in Fig. 7. Further, it is to be noted that, the untwisted blades used for current turbine prototype results in varying angles of attack along the blade span, maximum near the blade root and minimum at the blade tip. This will lead to span-wise flow variation with likelihood of flow separation (especially at low *TSR* values) at near-root sections (higher angle of attacks) without any flow separation for near-tip sections. These separated flow features can then propagate outwards along the blade span (Coriolis and centrifugal forces) toward the tip destabilizing the entire blade boundary layer. As the *TSR* value increases from 1.46 to 2.93, the percentage change in C_p from lowest blockage ratio (0.042) to highest blockage ratio (0.42) increases to 6%. Higher *TSR* values lead to larger variation of C_p with blockage, with maximum improvement of ~52% observed at *TSR* of 5.85. An interesting behavior was observed for *TSR* 4.39 and 5.85 cases: at blockage ratios below 0.2, *TSR* 4.39 case consistently showed higher performance as compared to *TSR* 5.85 case, but above solid blockage of 0.2, inflexion was observed with *TSR* 5.85 case performing better than *TSR* 4.39 case. Higher *TSR* cases (not presented here) showed even higher fluctuations in C_p vs. blockage curve with more than three inflexion points. This can be attributed to interaction of stronger wake blockage (due to free surface deformation) with solid blockage at these high *TSR* that leads to a complex coupled total blockage affecting turbine performance. For a given flow speed and blockage ratio, an increase in rotational speed leads to faster bypass flow, yielding higher C_p as plotted in Fig. 8a. However, for a given U and B, there exists a *TSR* at which a sudden jump in C_p is observed. The location of this inflexion point depends on flow velocity, rotational speed and blockage ratio. To confirm this hypothesis, additional experimental runs were performed with lab prototype at higher flow velocities. Experimental data was then corrected according to the blockage correction proposed by Bajah et al. [2]. Fig. 8b presents percentage change in power coefficient between corrected and measured (raw-experimental) data ($\%\Delta C_p = \frac{C_{P_{measured}} - C_{P_{corrected}}}{C_{P_{corrected}}} \times 100$). The data presented in Fig. 8b is from experimental runs for lab prototype corresponding to blockage ratio of 0.165. At his blockage ratio, no inflexion was observed for $U = 0.5$ m/s. However, for higher flow velocities of $U = 0.7$ m/s, the transition in C_p occurred at *TSR* of ~5 while for $U = 0.9$ m/s transition occurred early, at *TSR* of ~4.8. These points are marked by rectangles in Fig. 8b. Thus the inflexion behavior depends on flow velocity, rotational speed and blockage ratio which govern the flow velocities in the bypass flow and hence blockage effects.

4.4. Effect of boundary proximity on the turbine performance

When a turbine operates in a shallow channel as the present case, the flow in its proximity can be decomposed into two main components: (1) the flow passing through a stream-tube enclosing turbine rotation disc, which expands behind it forming a region commonly known as wake and, (2) a region called bypass region which is composed of remaining flow channel. We further decompose this bypass region into two zones: a flow region between free surface and rotor disc called *upper bypass* region and a region that lies between solid channel wall and rotor disc plane called *lower bypass* region. Such a distinction is required due to the very nature of widely different boundaries curtaining these regions. While the flow is tightly restricted by the channel solid wall from the bottom (which may be erodible or non-erodible), the upper free surface is deformable and does not offer strong restriction to wake expansion and bypass flow restoration. To understand the effect of boundary proximity (free surface and channel bottom wall) on turbine performance, experimental investigations were carried out by varying the tip clearance ratio (δh_U) from 0.03 to 0.73 (see Figs. 1 and 4). At each of these submersion depths, the rotational speed was varied from 30 to 300 RPM and torque values were recorded from submerged torque-thrust sensor at sampling rate of 500 samples per second. Experiments were repeated for three different flow speeds: 0.5 m/s, 0.66 m/s, and 0.73 m/s to understand how Reynolds number variation affects the turbine performance in presence of boundary proximity effects. Table 1 presents details of experimental runs carried out during current study.

4.4.1. Results of experimental investigation for boundary proximity effects

Fig. 9 presents results of experimental investigations where C_p is plotted against *TSR* for three different velocities: $U = 0.5$ m/s, 0.66 m/s and 0.73 m/s. This corresponds to turbine diameter based Reynolds number of 1.37×10^5, 1.8×10^5, and 2.0×10^5 respectively and blade chord based Reynolds number of 8.2×10^3, 10.8×10^3, and 12×10^3 respectively. For all cases, lowest performance was observed when turbine was at largest depth in our facility ($\delta h_U = 0.34$). With reduction in depth of immersion, improved performance was observed until $\delta h_U = 0.20$ for all cases except lower flow velocity of $U = 0.5$ m/s for which both $\delta h_U = 0.20$ and $\delta h_U = 0.55$ resulted in similar maximum C_p values. Thus, flow with higher Froude number (and Reynolds number) was more susceptible to boundary proximity effects. An increase in flow speed was observed to improve the turbine performance with maximum performance achieved at flow speed of 0.73 m/s and $\delta h_U = 0.20$. Moving the turbine away from channel bottom wall resulted in improved performance. This indicates that the close proximity of channel wall affects the flow field behind turbine and restricts wake expansion and reduces the turbine performance. This trend continued until h_U reached around 10% of channel depth ($\delta h_U = 0.2$) or 50% of turbine radius. Beyond this point, though the turbine was away from the solid channel wall, it was in close proximity of free surface leading to significant free surface deformation behind the rotor plane which interacted with turbine wake affecting its performance. This observation was also supported by transient CFD analysis results which is described in Section 4.4.2.

To identify the optimal depth of immersion for efficient turbine operation, experimental data for 0.5 m/s, 0.66 m/s and 0.73 m/s cases is re-plotted in Fig. 10 which presents power coefficient vs. tip clearance ratio curves at different *TSR* values. For the flow velocity of 0.5 m/s, for all *TSR* values, the turbine was found to perform at consistently higher C_p values over a wider range of tip clearance ratios: δh_U 0.2–0.5 (Fig. 10a). With increase in flow velocity (and corresponding rotational speed to maintain the *TSR*), optimum tip clearance depth (h_U) for turbine performance started to shift around 10% of the total channel depth ($\delta h_U = 0.2$, which also corresponds to 50% of turbine radius). For both 0.66 and 0.73 m/s flow velocities, maximum performance was observed when the tip clearance ratio was close to 20% (Fig. 10b and c). Any depths, lower than that induced strong free surface–wake interactions degrading the turbine performance. This indicates that the optimum installation depth for efficient MHkT operation should be such that, the turbine is submerged with rotor disc $0.5 \times R$ below

Table 1
Flow variables and turbine depth of immersions investigated during current experimental study.

Flow velocity U (m/s)	Re_{Chord} (U_{tip}, $TSR = 5$)	$Re_{Diameter}$	Froude number	Tip clearance ratio (δh_U)
0.5	4.1×10^4	1.37×10^5	0.2	0.03, 0.20,
0.66	5.4×10^4	1.8×10^5	0.27	0.55, 0.73
0.73	6.0×10^4	2.0×10^5	0.3	

the water surface and >1 × R above the channel bottom wall, where R denotes the turbine radius. Thus the optimum depth of water for MHkT installation should be greater than 3.5 times the turbine radius.

4.4.2. Results of transient CFD to investigate boundary proximity effects

A transient CFD analysis was performed to characterize the flow-field under a free surface, blocked flow environment shows presence of faster bypass regions and its dependence on boundary proximity. All simulations were run at a constant rotational speed of 200RPM and flow velocity of 0.5 m/s (TSR = 5.85). Four different cases were considered with tip clearance ratios (δh_U) of 0.73, 0.55, 0.20, and 0.03. Fig. 11 plots contours of stream-wise superficial water velocity normalized by free-stream velocity (U = 0.5 m/s) on a vertical plane passing through the turbine rotational axis for different tip clearance ratios after 5 s, i.e. 16.67 rotations. For all cases the wake region was observed to extend over entire downstream channel length (~8 × R). For higher depths of immersion (δh_U = 0.73, 0.55), tip vortex structures were observed in both upper and lower bypass regions. But with decreasing δh_U (0.20 and below), the tip vortices start to interact with the free surface and dissipate before propagating downstream the turbine. A significant free surface drop was observed behind the turbine rotation plane with free surface penetrating into the wake region (Fig. 11d). Fig. 11 also plots contours of stream-wise superficial water velocity normalized by free-stream velocity (U = 0.5 m/s) on a horizontal plane passing through the turbine rotational axis for different tip clearance ratios. Same color-map scale is used for both vertical and horizontal planes to elucidate difference in velocity variations between these two planes. The upper bypass region shows significantly higher velocities compared to lower bypass and bypass regions on either sides of turbine in horizontal planes. The contour plots on horizontal planes, as opposed to the vertical planes (in Fig. 11) show more symmetric wake and bypass region. Tip vortices and their merging with the main wake can be seen on either sides of turbine axis. Further, higher stream-wise flow velocities were observed for lower tip clearance ratio, which suggests presence of faster bypass flow for lower depths of immersion.

Fig. 11 also point out the effect of blockage and boundary proximity on flow upstream of the turbine. It is to be noted that for CFD simulations, the inlet velocity profile was defined to be uniform flow with stream-wise velocity of 0.5 m/s. But as the flow approaches the turbine plane, the presence of turbine was observed to modify the incoming flow as can be seen in Fig. 11. Similar observations were reported by Medici [11] who observed modifications to flow approaching turbine up to three diametrical distance upstream, which depended on turbine geometry, and operating conditions. Further the shape of incoming velocity profile was different for different surface proximity cases which indicates dependence of incoming velocity field on free surface proximity.

Fig. 12 presents wake expansion and its interaction with the deformable free surface for tip clearance ratios of δh_U = 0.73, 0.20 and 0.03. Contours of normalized instantaneous superficial stream-wise velocity after simulation time t = 5 s are plotted on various planes at downstream locations ranging from x = 0.1R to x = 5R. When the turbine was submerged deep inside the water channel (δh_U = 0.73), no significant wake-free surface interaction was observed (Fig. 12a). However when the turbine was placed in very close proximity of the free surface (δh_U = 0.03), significant free surface deformation was observed that interacted with wake and bypass flow resulting in modifications of downstream flow-structures. Such a close proximity of turbine to the free surface not only resulted in faster upper bypass flow but also a skewed wake as depicted in Fig. 12c. For δh_U = 0.20, flow acceleration was observed in the upper bypass region without any significant interaction with wake and lead to maximum turbine performance. For lower depths of immersions (δh_U = 0.20 and 0.03), the free surface drop behind turbine rotation plane provided additional obstruction to wake propagation and restoration process. This resulted in slower moving wake and faster upper bypass region as depicted in Figs. 11 and 12. For δh_U = 0.03 case, the wake is almost touching the free surface, so it appears (in Fig. 11) that there is no upper bypass region in a vertical plane aligned with the turbine axis. However, Fig. 12 which presents a more complete picture of the flow field shows flow acceleration in the upper bypass region (around wake) for both δh_U = 0.2 and δh_U = 0.03.

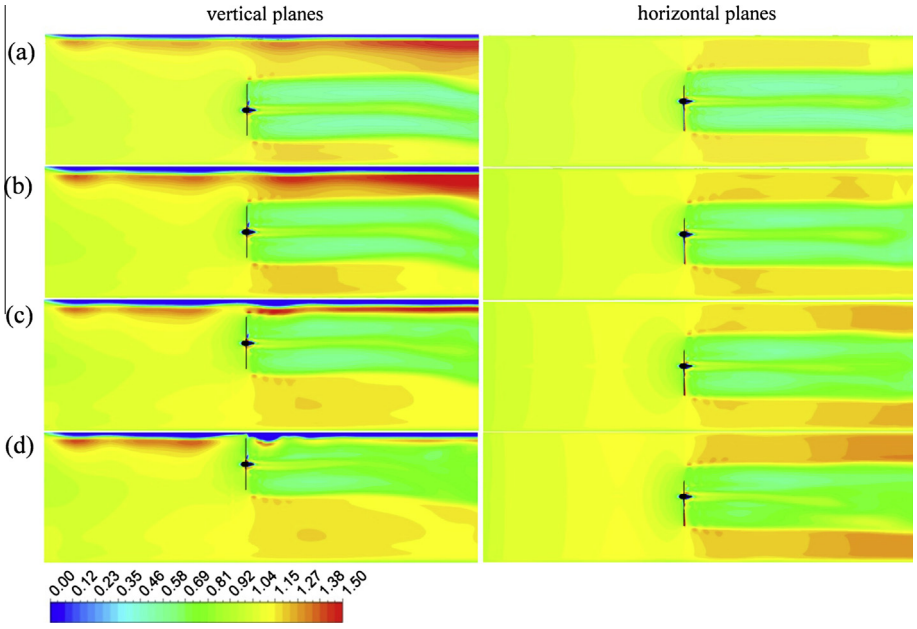

Fig. 11. Normalized stream-wise superficial (water) velocities on centerline vertical (left column) and horizontal (right column) planes after t = 5 s for (a) δh_U = 0.73 and (b) δh_U = 0.55, (c) δh_U = 0.20 and (d) δh_U = 0.03.

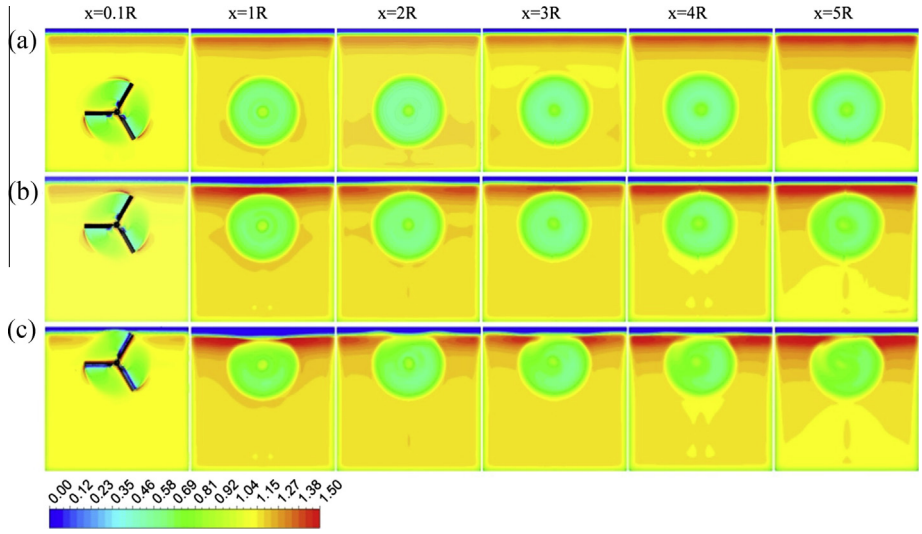

Fig. 12. Contours of normalized superficial velocity showing bypass and wake propagation at five downstream locations for tip clearance ratios of: (a) $\delta h_U = 0.73$ (b) $\delta h_U = 0.20$ and (c) $\delta h_U = 0.03$.

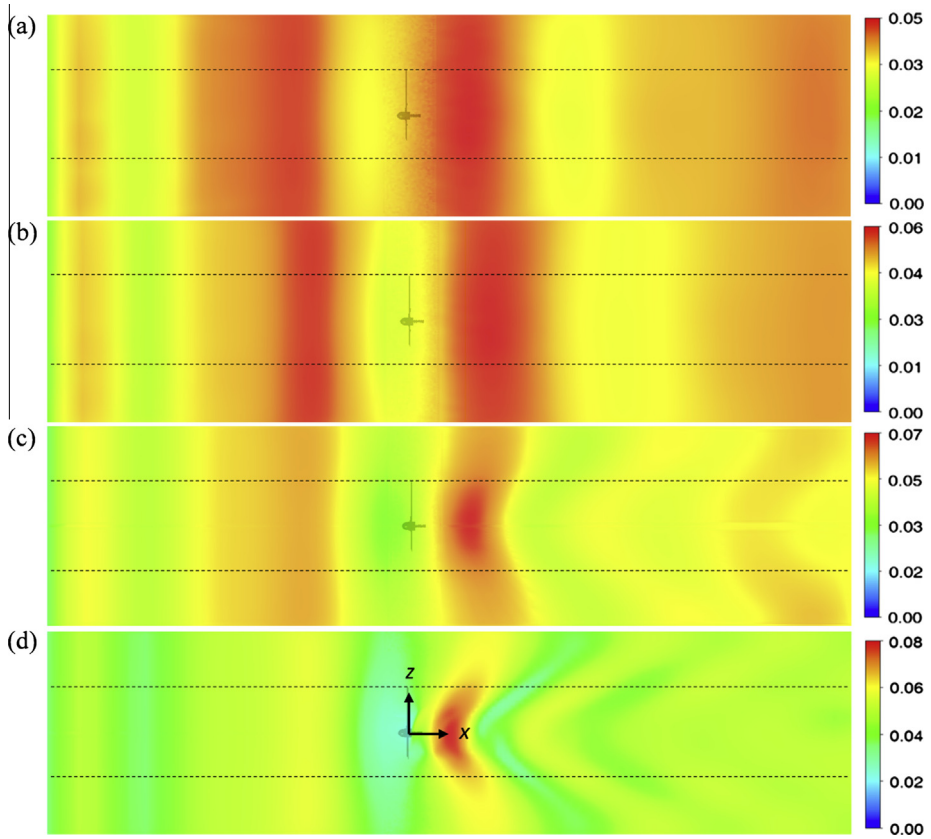

Fig. 13. Contours of free surface colored by normalized free surface drop ($\Delta h/h_1$) for tip clearance ratios of: (a) $\delta h_U = 0.73$ (b) $\delta h_U = 0.55$, (c) $\delta h_U = 0.20$ and (d) $\delta h_U = 0.03$. For relative location of the turbine, please refer to Fig. 4. (For interpretation of the references to colour in this figure legend, the reader is referred to the web version of this article.)

Thus a closer proximity of turbine to free surface retards wake propagation but accelerates the flow in upper bypass region compared to the case of a deeply submerged turbine. The free surface deformation complements the wake blockage effect (hence total blockage) and yields higher performance for $\delta h_U = 0.2$. But at $\delta h_U = 0.03$, wake starts strongly interacting with the upper bypass region leading to skewed wake and lower performance. It is to be noted here that, for all the tip clearance ratios considered during present study, CFD analysis did not show presence of any flow separation on turbine blades. This alludes to the fact that free surface deformation is the primary mechanism for increased or reduced performance at close proximity.

Furthermore, Fig. 11 also depicts the variation of free surface height along the length of the channel. The difference in heights (free surface drop) is more pronounced for $\delta h_U = 0.03$ case compared to $\delta h_U = 0.73$ case. This was also observed during

experimental investigations which showed presence of complex three dimensional structures and free surface drop behind turbine when it was operated in close proximity to free surface. A free surface drop up to 5–10% of channel depth was observed around $1 \times R$. behind turbine and this water surface drop was at its peak when turbine was operated at closest proximity to free surface. Fig. 13 obtained from transient simulations, shows free surface of water channel colored by normalized drop (free surface drop/channel depth) for various depths of immersions. Maximum free surface drop was observed when the turbine was in closest proximity of free surface ($\delta h_U = 0.03$). Further, shape of free surface drop curve was observed to be a function of depth of submersion. It is to be noted that contours in Fig. 13a–d are colored by normalized free surface drop ($\Delta h/h_1$), however the color-map scale for each case is chosen to elucidate the three dimensional structure of free surface drop for respective cases. When turbine was away from free surface, the free surface drop curve was a two dimensional structure showing distinct bands before and after the turbine rotation plane. But with closer proximity to free surface, these bands started to contract to a localized region. For $\delta h_U = 0.73$ a free surface drop of up to 5% of total channel depth was observed on downwind side of turbine rotation plane. With decreasing depth of submersion, free surface drop on upwind side of the turbine started diminishing relative to a localized three dimensional structure behind the turbine rotation plane. For $\delta h_U = 0.03$, a free surface drop up to 8% of total channel depth was observed when turbine was placed in close proximity of free surface.

5. Conclusion

Results of experimental and computational analysis for blockage effects, Reynolds number dependency and boundary proximity effects on flow-field and performance of a MHkT are presented. Experiments were carried out on a lab-scale MHkT at various flow velocities inside a 0.61 m × 0.61 m test section open surface recirculating water channel. CFD predictions based on rotating reference frame technique were in agreement with experimental data. CFD study was further extended to understand effect of flow Reynolds number and blockage ratio on turbine performance characteristics. Increasing flow velocity resulted in improved performance until 0.7 m/s beyond which C_p vs. *TSR* curve was found to be insensitive to Reynolds number change. Further, effect of solid blockage on turbine performance was analyzed by varying the size of fluid domain for lab prototype model. Blockage ratio below 10% did not show any appreciable effect on turbine performance characteristics. Increasing the solid blockage ratio from 10% to 42% resulted in widening the operating *TSR* range with up to ~35% improvement in power coefficient. Higher *TSR* values were found to exhibit higher blockage effects (higher percentage increase in C_p compared to unblocked case) due to faster rotational speed that lead to stronger wake and faster bypass flow. Further, to understand effect of surface proximity on turbine performance and flow-field, experiments were carried out with turbine at different depths of immersion. An improvement in performance was observed when turbine axis was moved away from the channel bottom (channel bottom wall to blade tip clearance > turbine radius). This trend continued until turbine was raised to tip clearance of half radius distance below the free surface, after which reduced performance was observed. Beyond this height, appreciable free surface drop was observed behind turbine rotational plane restricting the wake expansion and propagation process resulting in reduced performance. A three dimensional transient CFD analysis (with VOF formulation) that was performed for wake and near-free surface flow characterization revealed presence of three distinct flow regions behind turbine: wake, upper bypass and lower bypass region. The flow structures in these regions were found to depend strongly on proximity to channel bottom and free surface. For lower tip clearance ratios, a significant drop (up to 5–10% of channel depth) in free surface was also observed behind turbine with complex three dimensional flow structures that lead to a skewed wake affecting its expansion and restoration process. Further, a reduction in performance was observed when the turbine was operated close to the channel bottom wall. This can be attributed to two facts: first, the boundary layer and associated viscous effects at channel bottom wall that adversely affect the turbine performance, and second, absence of additional blockage due to free surface deformation that manifests when a turbine operates in proximity of a free surface. Since both distances were varied simultaneously, it is not possible to pin down the cause to the either of the cases described above. Free surface deformation and higher flow velocities in the upper bypass region (compared to lower bypass region) lead to an asymmetric wake behind the turbine. Transient CFD analysis at *TSR* = 5.85 for all depths of immersion studied during present work did not show any flow separation effects on turbine blades suggesting that, free surface deformation is the primary mechanism for increased or reduced performance of turbine operating in free surface proximity environment. In addition to wake and bypass regions behind the turbine, the presence of turbine in flow channel was observed to affect flow upstream of the turbine as well. Our experimental investigations suggest that for optimum performance, MHkT should be installed such that, turbine rotational disc is at least one radial distance away from the solid channel wall and half radial distance below the free surface.

References

[1] Stallard T, Collings R, Feng T, Whelan J. Interactions between tidal turbine wakes: experimental study of a group of three-bladed rotors. Phil Trans R Soc A 2013;371:20120159.
[2] Bahaj AS, Molland AF, Chaplin JR, Batten WMJ. Power and thrust measurements of marine current turbines under various hydrodynamic flow conditions in a cavitation tunnel and a towing tank. Renew Energy 2007;32:407–26.
[3] McTavish S, Feszty D, Nitzsche F. An experimental and computational assessment of blockage effects on wind turbine wake development. Wind Energy 2013.
[4] Consul CA, Willden RHJ, McIntosh SC. Blockage effects on the hydrodynamic performance of a marine cross-flow turbine. Phil Trans R Soc A 2013;371:20120299.
[5] Maskell EC. A theory of the blockage effects on bluff bodies and stalled wings in a closed wind tunnel. Defense Technical Information Center: Aeronautical Research Council London ed. Ft. Belvoir; 1963.
[6] Gould RWF. Wake blockage corrections in a closed wind tunnel for one or two wall-mounted models subject to separated flow. London: HMSO; 1969.
[7] Pope A. Wind-tunnel-boundary corrections. Wind-tunnel testing: John Wiley & Sons Inc.; 1954. p. 268–344.
[8] Vermeer LJ, Sorensen JN, Crespo A. Wind turbine wake aerodynamics. Prog Aerosp Sci 2003;39:467–510.
[9] Khan MJ, Bhuyan G, Iqbal MT, Quaicoe JE. Hydrokinetic energy conversion systems and assessment of horizontal and vertical axis turbines for river and tidal applications: a technology status review. Appl Energy 2009;86:1823–35.
[10] Whelan JI, Graham JMR, Peiro J. A free-surface and blockage correction for tidal turbines. J Fluid Mech 2009;624:281–91.
[11] Medici D, Ivanell S, Dahlberg JÅ, Alfredsson PH. The upstream flow of a wind turbine: blockage effect. Wind Energy 2011;14:691–7.
[12] Chen TY, Liou LR. Blockage corrections in wind tunnel tests of small horizontal-axis wind turbines. Exp Therm Fluid Sci 2011;35:565–9.
[13] Hu D, Du Z. Near wake of a model horizontal axis wind turbine. J Hydrodyn 2009;21:285–91.
[14] Hu H, Yang Z, Sarkar P. Dynamic wind loads and wake characteristics of a wind turbine model in an atmospheric boundary layer wind. Exp Fluids 2012;52:1277–94.
[15] Young YL, Motley MR, Yeung RW. Three-dimensional numerical modeling of the transient fluid–structural interaction response of tidal turbines. J Offshore Mech Arctic Eng 2010;132:011101.
[16] Kolekar N, Banerjee A. A coupled hydro-structural design optimization for hydrokinetic turbines. J Renew Sustain Energy 2013:5.
[17] Myers LE, Bahaj AS. The effect of boundary proximity upon the wake structure of horizontal axis marine current turbines. In: 27th International conference

on offshore mechanics and arctic engineering (OMAE 2008). The American Society of Mechanical Engineers; 2008.
[18] Bahaj AS, Myers LE, Rawlinson-Smith RI, Thomson M. The effect of boundary proximity upon the wake structure of horizontal axis marine current turbines. J Offshore Mech Arctic Eng 2011:134.
[19] Birjandi AH, Bibeau EL, Chatoorgoon V, Kumar A. Power measurement of hydrokinetic turbines with free-surface and blockage effect. Ocean Eng 2013;69:9–17.
[20] Garrett C, Cummins P. The efficiency of a turbine in a tidal channel. J Fluid Mech 2007;588:243–51.
[21] Houlsby GT, Draper S, Oldfield MLG. Application of linear momentum actuator disc theory to open channel flow. Department of Engineering Science, University of Oxford; 2008.
[22] Lartiga C, Crawford C. Actuator disk modelling in support of tidal turbine rotor testing. In: 3rd Int Conf on Ocean Energy. Bilbao, Spain; 2010.
[23] Sun X, Chick JP, Bryden IG. Laboratory-scale simulation of energy extraction from tidal currents. Renew Energy 2008;33:1267–74.
[24] Bai X, Avital EJ, Munjiza A, Williams JJR. Numerical simulation of a marine current turbine in free surface flow. Renew Energy 2014;63:715–23.
[25] Zhou JW, Wang DZ. Simulation of tidal stream turbine working near free surface. Appl Mech Mater 2013;361–3:291.
[26] Lee JH, Park S, Kim DH, Rhee SH, Kim M-C. Computational methods for performance analysis of horizontal axis tidal stream turbines. Appl Energy 2012;98:512–23.
[27] Myers LE, Bahaj AS. Experimental analysis of the flow field around horizontal axis tidal turbines by use of scale mesh disk rotor simulators. Ocean Eng 2010;37:218–27.
[28] Hirt CW, Nichols BD. Volume of fluid (VOF) method for the dynamics of free boundaries. J Comput Phys 1981;39:201–25.
[29] ANSYS CFX 14 Theory guide. ANSYS, Inc.; 2011.
[30] Mukherji SS, Kolekar N, Banerjee A, Mishra R. Numerical investigation and evaluation of optimum hydrodynamic performance of a horizontal axis hydrokinetic turbine. J Renew Sustain Energy 2011;3:063105.
[31] Wilcox DC. Turbulence modeling for CFD. 3rd ed. La Canada, CA: DCW Industries; 2006.
[32] Menter FR, Kuntz M, Langtry R. Ten years of industrial experience with the SST turbulence model. Turbul, Heat Mass Transfer 2003;4. Hanjalic K, Nagano Y, Tummers M (editors). Begell House, Inc.; 2003. p. 625–32.
[33] Anderson JD. Computational fluid dynamics: the basics with applications. McGraw Hill International; 1995.
[34] Kline SJ, McClintock FA. Describing uncertainties in single-sample experiments. Mech Eng 1953;75:3–8.